

# AnTKV: Anchor Token-Aware Sub-Bit Vector Quantization for KV Cache in Large Language Models

Zeyu Li<sup>♣\*</sup> Chuanfu Xiao<sup>♡,§</sup> Yang Wang<sup>◇,§</sup> Xiang Liu<sup>♣</sup> Zhenheng Tang<sup>♣</sup>  
 Baotong Lu<sup>◇</sup> Mao Yang<sup>◇</sup> Xinyu Chen<sup>♣</sup> Xiaowen Chu<sup>♣,♣,§</sup>

<sup>♣</sup> DSA Thrust, The Hong Kong University of Science and Technology (Guangzhou)

<sup>♡</sup> PKU-Changsha Institute for Computing and Digital Economy

<sup>◇</sup> Microsoft <sup>♣</sup> The Hong Kong University of Science and Technology

## Abstract

Quantization has emerged as an effective and lightweight solution to reduce the memory footprint of the KV cache in Large Language Models (LLMs). Nevertheless, minimizing the performance degradation caused by ultra-low-bit KV cache quantization remains a significant challenge. We observe that quantizing the KV cache of different tokens has varying impacts on the quality of attention outputs. To systematically investigate this phenomenon, we perform forward error propagation analysis on attention and propose the Anchor Score (AnS) that quantifies the sensitivity of each token’s KV cache to quantization-induced error. Our analysis reveals significant disparities in AnS across tokens, suggesting that preserving a small subset with full precision (FP16) of high-AnS tokens can greatly mitigate accuracy loss in aggressive quantization scenarios. Based on this insight, we introduce AnTKV, a novel framework that leverages Anchor Token-aware Vector Quantization to compress the KV cache. Furthermore, to support efficient deployment, we design and develop a triton kernel that is fully compatible with FlashAttention, enabling fast online Anchor Token selection. AnTKV enables LLaMA-3-8B to handle context lengths up to 840K tokens on a single 80GB A100 GPU, while achieving up to 3.5x higher decoding throughput compared to the FP16 baseline. Our experiment results demonstrate that AnTKV matches or outperforms prior works such as KIVI, SKVQ, KVQuant, and CQ under 4-bit settings. More importantly, AnTKV achieves significantly lower perplexity under ultra-low-bit quantization on Mistral-7B, with only 6.32 at 1-bit and 8.87 at 0.375-bit, compared to the FP16 baseline of 4.73.

## 1 Introduction

LLMs have attracted much attention due to their strong capability in natural language processing and other artificial intelligence tasks [1, 2, 3, 4, 5]. With the rapid development in recent years, LLM can manage increasingly larger context lengths ranging from hundreds of thousands to millions of tokens, and its broadening scope allows LLM to tackle more complex tasks [6, 7, 8, 9]. However, these models, which are typically built on decoder-based transformer architectures, generate tokens recursively during inference, thus leading to a large accumulation of the KV cache as the context length [10, 11, 12] and batch size increases [13]. The large memory footprint of the KV cache presents a significant challenge. For long-context inference, such as LLaMA-3’s 128K context length, the KV cache can consume several gigabytes of memory, nearly matching the model’s weights. This challenge is even greater for models like Gemini, which handle contexts up to a million tokens.

\*Part of the work was done when Zeyu interned at Microsoft.

§ Correspondence Authors.

Moreover, LLM-RAG systems [14] pre-generate and store KV caches. However, the excessive size of these caches presents a significant challenge for storage.

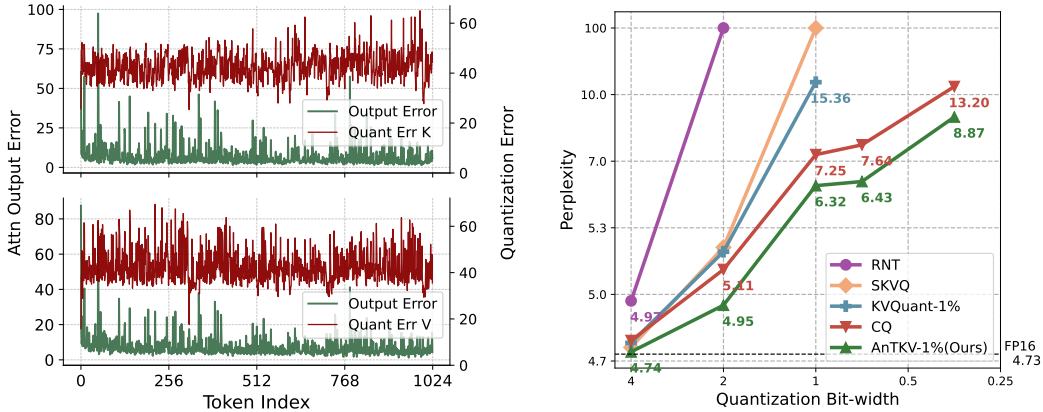


Figure 1: Self-attention output error when quantizing the KV cache of Mistral-7B to 1-bit.

Figure 2: The perplexity of Mistral-7B on the Wikitext2 under different bit-widths.

To address the growing KV cache, various optimization strategies have been proposed [15, 16, 17, 18, 19, 5], with quantization emerging as a prominent solution. Quantization approaches fall into two main categories: scalar quantization (SQ) and vector quantization (VQ). SQ compresses the KV cache by mapping floating-point values to fixed low-bit representations [19, 20, 21], but the minimum 1-bit requirement limits its compression to 1/16 on FP16. In contrast, VQ maps high-dimensional vectors to a finite codebook [22, 23], capturing intra-vector correlations. This enables higher compression rates and better preserves representational fidelity, especially under ultra-low-bit regimes.

During the LLM inference, different tokens have different effects on the accuracy of LLMs, so it is unreasonable to treat all tokens equally in VQ methods. To illustrate this, we quantize the KV cache of Mistral-7B [24] to 1-bit using VQ, and Figure 1 shows the impact of KV quantization on the self-attention output error within layer 31. It reveals that even in the absence of tokens with exceptionally large quantization errors, a few tokens (**Anchor Tokens**) can still introduce substantial deviations in the output of the self-attention operator. **Therefore, measuring the importance of tokens during inference can further explore the performance potential of VQ methods for compressing the KV cache.**

To this end, we introduce **Anchor Score** (AnS), a metric derived from forward error analysis, to quantify each token’s impact on the output. Leveraging AnS, we propose **AnTKV**, a novel framework that employs anchor token-aware VQ for KV cache compression. AnTKV mitigates quantization-induced degradation through a two-stage design: offline token-aware centroids learning and online anchor token selection. In the offline stage, the framework performs the token-aware weighted k-means clustering to generate centroids. During the online stage, it computes the AnS for each request to identify anchor tokens that significantly contribute to output error and selectively retains their FP16. Moreover, to ensure efficiency, we expose key intermediate variables from FlashAttention [25] and integrate a lightweight GPU kernel for AnS computation during inference, enabling efficient runtime anchor token selection.

To validate AnTKV’s effectiveness, we conduct extensive experiments across various quantization bit-widths on a range of LLMs, including LLaMA-2/3 [26, 27] and Mistral-7B [24] family. As depicted in Figure 2, AnTKV consistently achieves better performance across a wide spectrum of bit-widths, from 4-bit down to 0.375-bit. On Wikitext2 with Mistral-7B, AnTKV achieves a perplexity of 6.32 at 1-bit, a reduction of 0.93 compared to CQ (7.25) [23], and substantial 9.04 over KVQuant-1% (15.36) [21]. Even at an aggressive 0.375-bit, AnTKV further lowers perplexity to 8.87, surpassing CQ (13.20) by 4.33. Enabled by the efficient implementation of AnS, AnTKV scales to extremely long contexts. On LLaMA-3-8B, it supports up to 840K context length under 0.375-bit on a single A100-80GB GPU. During decoding, AnTKV increases the maximum batch size by 3.3x and improves throughput by 3.4x at 1K context length compared to FP16. More experiments that demonstrate the performance advantages of the proposed AnTKV are in Section 4.

To summarize, we make the following contributions in this work.

- We conduct an error analysis of the self-attention, and introduce AnS to quantify the importance of tokens. With AnS, we can identify anchor tokens that significantly impact the accuracy of LLMs. Based on AnS, we present a novel token-aware VQ method, namely AnTKV, to compress the KV cache in LLM inference.
- To ensure efficiency, we design a custom GPU kernel for computing AnS in the online stage that is compatible with FlashAttention. With the high-performance implementation of AnS, AnTKV can support up to 840K context length on a single GPU.
- We deploy the proposed AnTKV in LLaMA-2/3 and Mistral-7B family, numerical results show that AnTKV has a significant performance improvement under various quantization bit-widths.

## 2 Background and Related Works

### 2.1 Transformer and Attention

The transformer block has become the fundamental architecture of LLMs; it consists of a fully connected feed-forward layer and a self-attention layer. The self-attention layer enables the model to capture connections among tokens within the context and serves as the critical component of the transformer block. Specifically, it maps a query ( $Q$ ) and a set of KV pairs ( $K$  and  $V$ ) to an output, i.e.,

$$\text{Attn}(Q, K, V) = \text{Softmax}\left(\frac{QK^T}{\sqrt{d}}\right)V \quad \text{with } Q, K, V \in \mathbb{R}^{n \times d},$$

where  $\text{Softmax}(\cdot)$  is the softmax operator. Since position information is crucial in LLMs, Rotary Position Embedding (RoPE) [28] is a widely used technique for encoding it into query and key vectors [29], which is denoted as  $\tilde{Q}$  and  $\tilde{K}$  in this paper. With RoPE, the attention score  $A$  is rewritten as  $\text{Softmax}\left(\frac{\tilde{Q}\tilde{K}^T}{\sqrt{d}}\right)$ , and its  $L_p$  “entry-wise” matrix norm is defined as  $\left(\sum_{i,j} |A_{i,j}|^p\right)^{1/p}$ .

Other notations used in this work, such as the Kronecker product, the Hadamard product, and the row-by-row vectorization are denoted as  $\otimes$ ,  $\odot$ , and  $\text{Vec}(\cdot)$ , respectively.

### 2.2 Memory Constraints in LLM Inference

During the process of LLM inference, the key and value generated at prefill and each decoding step are stored to avoid redundant computation. The KV cache is repeatedly accessed in subsequent steps to compute attention over the full context seen so far, significantly accelerating autoregressive decoding. In a multi-turn conversation, the KV cache from previous turns can also be reused during the prefill stage to further reduce latency. The state-of-the-art open-source and closed-source LLMs, like LLaMA-3.1-8B [27] and Gemini 1.5 Pro [3], now handle much longer context lengths, up to 128K and 2 million tokens, respectively. This increase in context length [12, 9] causes the GPU memory used for the KV cache in LLM inference to even exceed the models’ size. The rapid growth of KV cache greatly limits the deployment of LLMs with long context. Quantizing the KV cache directly optimizes this by maintaining key-value information and cutting memory costs substantially, thus enhancing the efficiency of LLM inference.

### 2.3 Related Works

**KV cache quantization** A variety of KV cache quantization methods have been developed to address the memory bottleneck in long-context LLMs [19, 20, 21, 23, 30]. KIVI [19] reduces quantization error via per-channel key quantization combined with a sliding window strategy to emphasize locally relevant tokens. SKVQ [20] further explores this direction by introducing channel reordering and clipping to improve low-bit quantization. In contrast, KVQuant [21] adopts a different design by quantizing pre-RoPE keys using non-uniform quantization and selectively preserving a small fraction of full-precision KV entries to mitigate accuracy loss. CQ [23] adopts a VQ-based approach, aiming to exploit cross-channel correlations to further compress the KV cache.

**KV cache compression** Beyond quantization, the field of LLMs is actively exploring several advanced methods for KV cache compression. Sparse attention are designed to achieve compression by

selectively computing attention over a reduced set of tokens [31, 32, 10, 15, 16, 33]. However, a significant limitation lies in the inherent complexity of designing and optimizing their sparsity patterns. This often necessitates task-specific or data-driven heuristics, which can severely constrain their efficient generalization across diverse model architectures and datasets. Token merge, as a variant of sparse attention, merges the KV cache of similar tokens during inference to reduce memory usage [18, 34]. Retrieval-based methods [17, 35, 36] compress KV caches by retrieving relevant historical context for each query and are effective in tasks like RAG or document retrieval. However, they often lose substantial KV information, making them less suitable for general-purpose LLM inference.

**Model Compression** Many model compression techniques closely align with KV cache compression in both goals and underlying methodologies. GPTQ [37] utilizes calibration set to reduce quantization induced degradation, while SmoothQuant [38] and AWQ [39] minimize output error from the perspective of error propagation analysis. VQ-based methods such as VPTQ [40] and QUIP# [41] further enhance compression fidelity through residual VQ and Hadamard transform. Additionally, system-level frameworks like Atom [42] and QServe [43] jointly optimize model and KV cache quantization, achieving end-to-end acceleration under low-bit quantization. Other works, such as Pruner-Zero [44] and Parzc [45], explore how to sparsify model weights while preserving model performance. Systems like FlashLLM [46] and Spinfer [47] leverage the model sparsity to accelerate inference.

### 3 Methodology

Previous works on quantifying the KV cache typically do not distinguish the importance of individual tokens, but assume that all tokens contribute equally to attention accuracy, or they adopt a simpler strategy of only preserving designated sink tokens. However, our 1-bit VQ experiment on Mistral-7B contradicts this, unveiling a previously unaddressed aspect in KV cache quantization: a small subset of tokens provokes disproportionately large perturbations in the self-attention outputs. This divergence reveals a new opportunity for KV cache quantization. Instead of uniform application, the precision of quantization should correspond to each token’s individual importance. Specifically, if we identify and preserve a subset of high-impact tokens in FP16, we can unlock a far better memory–accuracy trade-off.

Inspired by this, we present a novel token-aware VQ method for KV cache compression, namely, AnTKV. In AnTKV, we adopt a two-stage design: offline token-aware centroids learning (see Figure 3(a)) and online anchor token selection (see Figure 3(b)), the key of which lies in how to measure the importance of tokens. In the offline stage, we perform a weighted k-means clustering to produce centroids in VQ, and the gradient corresponding to each token is used as weights. In the online stage, to reduce the output error caused by quantization, we select tokens with both higher  $\text{Err}_{\text{quant}}$  and AnS, i.e. anchor tokens, and keep them at FP16. Additionally, since applying RoPE disrupts the consistency of channel-wise magnitudes in  $\mathbf{K}$  (see Appendix A for an illustrative example), which exhibits large inter-cluster distances and small intra-cluster variances, leading to large quantization error, the pre-RoPE strategy with the same as [21] is used in AnTKV.

#### 3.1 Offline Token-Aware Centroids Learning

The offline stage aims to learn centroids by aggregating KV cache from general calibrations. Specifically, each row (per token) of  $\mathbf{K}$  and  $\mathbf{V}$  is divided into several sub-vectors, then using k-means to cluster them, and only the centroids are stored. To integrate the importance of tokens, we introduce the weighted k-means instead of classical k-means for the offline centroids learning.

From the perspective of accuracy, we hope that the errors caused by quantizing  $\mathbf{K}$  and  $\mathbf{V}$  will not affect the accuracy of LLMs as much as possible. Mathematically, it can be formulated as

$$\min_{\mathbf{C}^k \in \mathbb{R}^{c^k \times d}} |L(\mathbf{K}, \mathbf{V}) - L(\text{vq}(\mathbf{K}), \text{vq}(\mathbf{V}))|, \quad (1)$$

where  $c^k$  is the number of clusters, and  $\mathbf{C}^k$  is the matrix consisting of centroids. By the first-order Taylor series expansion, we have

$$L(\mathbf{K}, \mathbf{V}) - L(\text{vq}(\mathbf{K}), \text{vq}(\mathbf{V})) \approx \sum_j \left( \left\langle \frac{\partial L}{\partial \mathbf{K}_{j,:}}, \mathbf{K}_{j,:} - \text{vq}(\mathbf{K}_{j,:}) \right\rangle + \left\langle \frac{\partial L}{\partial \mathbf{V}_{j,:}}, \mathbf{V}_{j,:} - \text{vq}(\mathbf{V}_{j,:}) \right\rangle \right), \quad (2)$$

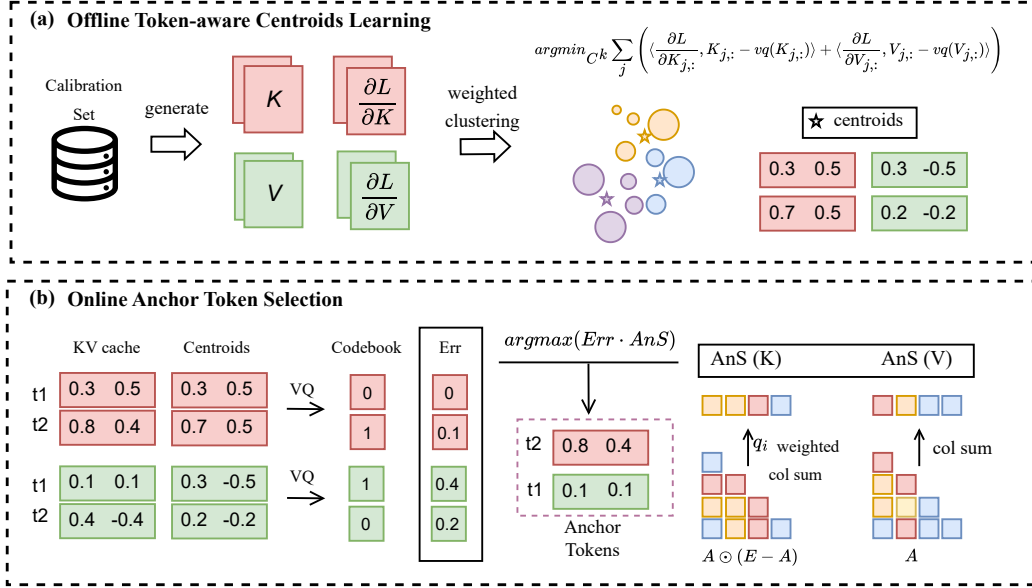


Figure 3: The overview of AnTKV. (a) In the offline stage, we perform token-aware centroid learning to obtain the centroids. (b) In the online stage, we apply VQ using centroids and compute the AnS. Then identify the top- $k$  anchor tokens with the highest product of VQ error and AnS, and retain them in full-precision to preserve anchor model performance.

where  $\frac{\partial L}{\partial K_{j,:}}$  and  $\frac{\partial L}{\partial V_{j,:}}$  are the gradient of the loss function  $L(\cdot)$  with respect to  $K_{j,:}$  and  $V_{j,:}$ , i.e., the  $j$ th row of  $K$  and  $V$  that correspond to the  $j$ th token. From (1) and (2), the weighted k-means clustering with gradients as weights is essentially to find a clustering strategy that minimizes the error caused by KV quantization. This also explains the effectiveness of the weighted k-means clustering used in this stage.

### 3.2 Online Anchor Token Selection

In the online stage, the gradient can no longer be used as AnS due to prohibitive memory and computational costs under real-time constraints. To this end, we here give the error propagation analysis of the self-attention (i.e.,  $\text{Attn}$ ). Specifically, the error propagation analysis is based on the perturbation bound of  $\text{Attn}$  that is related to each row of  $K$  and  $V$ ; see Theorem 3.1 (see Appendix B for proof).

**Theorem 3.1.** Let  $\delta K$  and  $\delta V$  be the error perturbation terms corresponding to  $K$  and  $V$  respectively, and satisfy

$$\|\delta K\|_{L_1} \ll \|K\|_{L_1} \quad \text{and} \quad \|\delta V\|_{L_1} \ll \|V\|_{L_1}.$$

Then we have

$$\begin{aligned} & \|\text{Attn}(Q, K + \delta K, V) - \text{Attn}(Q, K, V)\|_{L_1} \\ & \lesssim \sum_j \sum_i \left\| \left( V^\top \text{Diag}(A_{i,:}) (\mathbf{I}_n - e A_{i,:}) \right)_{:,j} \right\|_{L_1} \|Q_{i,:}\|_{L_2} \|\delta K_{j,:}\|_{L_1} \end{aligned} \quad (3)$$

and

$$\|\text{Attn}(Q, K, V) - \text{Attn}(Q, K, V + \delta V)\|_{L_1} \leq \sum_j \|A_{:,j}\|_{L_1} \|\delta V_{j,:}\|_{L_1}, \quad (4)$$

where  $e \in \mathbb{R}^n$  is a vector whose entries are all 1.

We remark that the error propagation factors corresponding to  $K_{j,:}$  and  $V_{j,:}$  given in Theorem 3.1 can be regarded as the upper bound of the gradient of the self-attention operator related to  $K_{j,:}$  and  $V_{j,:}$ .

The computation involving  $\mathbf{K}$  in Theorem 3.1 entails substantial overhead, rendering it impractical for use during online inference. To address this, we propose a simplified variant that excludes the contribution of  $\mathbf{V}$  to the quantization error of  $\mathbf{K}$ . By this simplification, we obtain the following reformulation. A detailed evaluation of the effectiveness of AnS is provided in Appendix C.

$$\text{AnS}(\mathbf{K}_{j,:}) = \sum_i \mathbf{A}_{i,j}(1 - \mathbf{A}_{i,j}) \cdot \|\mathbf{Q}_{i,:}\|_2 \quad (5)$$

During the prefill phase, AnS serves as an effective metric to identify anchor tokens that preserve critical contextual information by measuring their impact on attention outputs. In contrast, although AnS can still be computed during decoding, the anchor token it identifies may have already been quantized during prefill, preventing the preservation of its FP16 value for reducing accumulated errors. An important observation is that  $\mathbf{A}$  and  $\mathbf{A} \odot (\mathbf{E} - \mathbf{A})$  exhibit strong locality during decoding (see Appendix D), with anchor tokens primarily concentrated at the beginning and end of the sequence. In particular, the beginning tokens—referred to as sink tokens—are almost always identified as anchor tokens during prefill, indicating that our method effectively handles sink tokens. Motivated by this locality, we adopt a sliding window approximation of AnS during decoding.

### 3.3 Implementation

For the offline stage, the gradient of  $\mathbf{K}$  and  $\mathbf{V}$  is used as a weight to learn centroids. We implement it with a custom LinearWithAct to capture KV cache and corresponding gradients. Subsequently, we employ the weighted K-Means provided by cuML to perform efficient clustering.

For the online stage, AnS is derived from the error propagation factor given in Theorem 3.1 and (5). We design and implement a dedicated GPU kernel using Triton to efficiently compute it in conjunction with FlashAttention, enabling long-context inference. Since AnS requires reduction operations over the attention score matrix  $\mathbf{A}$  and its transformed form  $\mathbf{A} \odot (\mathbf{E} - \mathbf{A})$  along query (column-wise), directly fusing its computation into FlashAttention is impossible. To preserve the efficiency of FlashAttention, we decouple the AnS computation and execute it immediately afterward. To support this design, we extend FlashAttention to preserve three auxiliary tensors: the  $L_2$  norm of each query vector, the key-wise (row-wise) sum, and the key-wise maximum of the matrix  $\mathbf{Q}\mathbf{K}^T$ . These additional outputs enable efficient reconstruction of the attention scores and allow AnS to be computed with minimal overhead. More details about the implementation are described in Algorithm 1 of Appendix E.

## 4 Experiments

In this section, we compare the performance of AnTKV with existing KV quantization methods through extensive experiments. The experimental setup, including models, benchmark datasets, evaluation metrics, and selected baselines, is as follows.

**Models, Datasets, Metrics, and Parameter Settings.** To validate the effectiveness of AnTKV in KV cache quantization and ensure the generality of results, we evaluate five representative models from the LLaMA and Mistral families: LLaMA-2-7B, LLaMA-3-8B, LLaMA-3-8B-Instruct, Mistral-7B, and Mistral-7B-Instruct-v0.3. We use 128 samples of length 2048 from the WikiText2-v1 training set as the calibration. Perplexity is evaluated on WikiText-2 and C4, while zero-shot accuracy on MMLU [48], ARC-C [49], MathQA [50], and PIQA [51] is used to assess understanding and reasoning. Long-context performance is measured using LongBench [11]. For perplexity and zero-shot benchmarks, quantized KV cache is employed for attention. In LongBench, the FP16 KV cache is first utilized to compute attention outputs, before quantization is applied.

**Baselines.** We compare AnTKV against full-precision (FP16) and several representative KV cache quantization methods, including KIVI [19], SKVQ [20], KVQuant-1% [21], and CQ [23]. SKVQ uses a group size of 64 and 5 sink tokens [31], while KVQuant retains four sink tokens. In the absence of reported results, we reproduced CQ, guided by the methodology described in their paper and our best understanding. For VQ settings, we adopt the notation “*dncm*”, with configurations: 4-bit (d2m256), 2-bit (d4m256), 1-bit (d8m256), 0.75-bit (d16m4096), and 0.375-bit (d32m4096).

Due to the constraints of implementation, KIVI is excluded from perplexity and reasoning evaluation, and KVQuant is omitted from reasoning evaluation.

#### 4.1 Perplexity Results

Perplexity is a standard metric that is widely used to evaluate the quality of the output of LLMs, with lower values indicating better performance. The perplexity results for different KV quantization approaches on WikiText-2 and C4 are presented in Table 1. The results in this table indicate that the proposed AnTKV consistently achieves competitive or superior perplexity across various bit-widths and model architectures. Under 4-bit and 2-bit quantization, AnTKV achieves competitive or superior performance compared to existing approaches. In the 1-bit and sub-bit regimes, AnTKV significantly outperforms all baselines. It is worth mentioning that on the C4 dataset under sub-bit quantization, the baseline methods exhibit extremely high perplexity due to anchor tokens not being well captured by fixed centroids. Thanks to effective AnS design and innovative Anchor Token selection, AnTKV substantially reduces perplexity, e.g., from 66.28 to 14.42 (LLaMA-3-8B, 0.75-bit).

Table 1: The evaluations are conducted using each model’s maximum context length, specifically 4096 for LLaMA-2-7B and 8192 for LLaMA-3-8B and Mistral-7B. "Ours" refers to our method (AnTKV) without using any anchor tokens, while Ours-1% denotes AnTKV where 1% of the tokens are treated as anchor tokens and retained in FP16. For simplicity, the reported bit-widths do not consider the effect of centroids.

Dataset	Bit	LLaMA-2-7B		LLaMA-3-8B		Mistral-7B	
		WikiText2	C4	WikiText2	C4	WikiText2	C4
Baseline	16	5.12	6.63	5.54	7.10	4.73	5.66
RTN	4	5.66	7.31	7.89	8.79	7.34	5.91
SKVQ		5.16	6.67	5.64	7.19	4.97	5.68
KVQuant-1%		<b>5.13</b>	<b>6.65</b>	<b>5.56</b>	<b>7.12</b>	4.78	5.72
CQ		5.14	6.67	5.58	7.84	4.79	5.74
Ours		5.18	6.76	5.61	7.69	4.76	5.69
Ours-1%		5.15	6.68	5.59	7.16	<b>4.74</b>	<b>5.67</b>
RTN	2	4708	4708	2841	2113	573	477
SKVQ		5.54	7.21	6.73	8.31	5.21	6.14
KVQuant-1%		5.49	<b>7.02</b>	6.11	<b>7.65</b>	5.19	6.10
CQ		5.42	7.23	6.09	18.71	5.11	6.17
Ours		5.51	7.45	6.10	16.96	5.08	6.18
Ours-1%		<b>5.34</b>	<b>7.02</b>	<b>5.97</b>	7.68	<b>4.95</b>	<b>5.97</b>
SKVQ	1	12643	12819	108879	86426	3524	2741
KVQuant-1%		21.55	51.84	14.80	13.95	15.36	14.24
CQ		7.75	12.49	9.56	81.74	7.25	9.89
Ours		7.92	13.01	9.62	74.47	7.32	10.51
Ours-1%		<b>6.50</b>	<b>9.40</b>	<b>8.51</b>	<b>12.51</b>	<b>6.32</b>	<b>8.44</b>
CQ		0.75	8.39	14.32	11.18	72.05	7.64
Ours	8.21		14.27	10.41	66.28	7.41	11.72
Ours-1%	<b>6.55</b>		<b>9.75</b>	<b>8.97</b>	<b>14.42</b>	<b>6.43</b>	<b>9.08</b>
CQ	0.375	14.82	33.59	22.80	103.5	13.20	26.34
Ours		13.37	30.51	17.70	103.5	11.65	23.98
Ours-1%		<b>8.75</b>	<b>15.86</b>	<b>13.41</b>	<b>34.08</b>	<b>8.87</b>	<b>14.87</b>

#### 4.2 Understanding and Reasoning Benchmark

To ensure that AnTKV exhibits broad understanding and reasoning capabilities, we evaluate its performance on four representative benchmarks: MMLU, ARC-Challenge, PIQA, and MathQA, using both LLaMA-8B-Instruct and Mistral-7B-Instruct. These benchmarks respectively assess multi-domain knowledge reasoning (MMLU), complex question answering (arc\_challenge), commonsense reasoning (PIQA), and mathematical problem-solving (MathQA). Figure 4 illustrates the comparison results of AnTKV with SKVQ and CQ. Similarly, it can be seen that AnTKV consistently outperforms

SKVQ and CQ across all four benchmarks under low-bit quantization, especially at 1-bit and sub-bit levels.

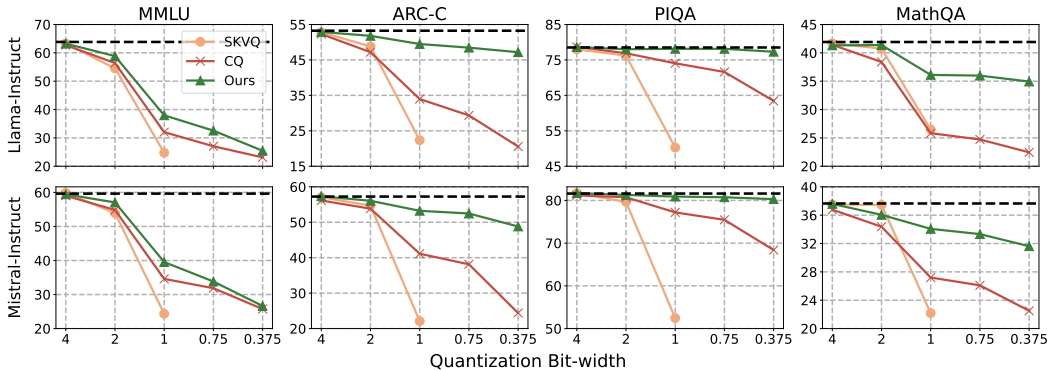


Figure 4: Understanding and Reasoning ability evaluation accuracy results on MMLU, ARC-C, PIQA, and MathQA under different quantization bit-widths.

### 4.3 Long-Context Benchmark

To validate the effectiveness of AnTKV in handling long-context, We conduct several experiments on the LLaMA-8B-Instruct model using the LongBench benchmark, a diverse collection of tasks such as question answering, retrieval, and summarization, designed to systematically evaluate long-context understanding in language models. We report results on eleven representative sub-tasks from LongBench, along with averaged performance. Due to alignment issues of KIVI and SKVQ, we exclude the triviaqa and gov\_report sub-tasks from the comparison. As shown in Figure 5, AnTKV preserves nearly FP16 at 4- and 2-bit quantization across almost all tasks. At the 1-bit quantization, the performance of KIVI and SKVQ has a significant drop. In contrast, AnTKV and CQ still maintain a relatively high accuracy. To further investigate the robustness under aggressive compression, we compare AnTKV and CQ in both sub-bit levels. Figure 5 shows that AnTKV consistently outperforms CQ. Notably, when quantizing down to 0.375-bit, AnTKV maintains a tolerable performance degradation, with the average score dropping from 46.2 to 34.5.

### 4.4 Efficiency

In this experiment, we evaluate the efficiency of our AnTKV implementation against the FlashAttention-accelerated FP16 baseline on LLaMA-3-8B using a single A100-80GB GPU. As shown in Figure 6, AnTKV substantially extends the maximum context length from 128K to 384K. In long-context scenarios, we observe that intermediate activations consume a significant portion of memory. By applying a series of in-place operations, AnTKV ultimately supports up to 810K tokens under 1-bit quantization and 840K under 0.375-bit quantization. More importantly, AnTKV sustains low memory consumption while maintaining acceptable latency. Under 1-bit quantization, a noticeable increase in prefill latency is observed only at the 128K context length, which represents the upper limit supported by most current models. It is observed that 0.375-bit quantization introduces higher latency than its 1-bit. This increase in latency arises from the use of a larger number of centroids, which are employed to enhance model accuracy.

To evaluate decoding efficiency, we evaluate the throughput of AnTKV under a fixed context length of 1K tokens. As shown in Figure 7, AnTKV supports significantly larger batch sizes compared to the baseline method. By substantially reducing KV cache access, it improves throughput across all bit-widths. Particularly, the maximum throughput reaches 3.5x that of the baseline method under 1-bit quantization.

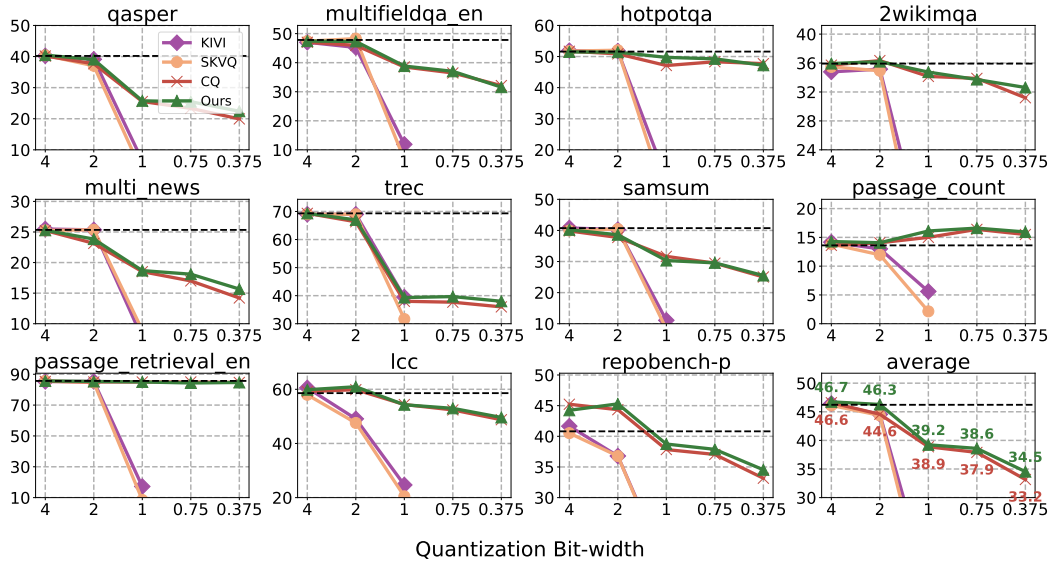


Figure 5: The evaluation accuracy results on LongBench under different KV cache quantization bit-widths.

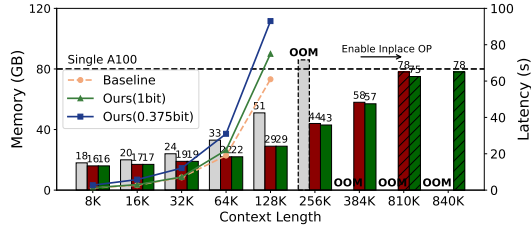


Figure 6: Memory and latency comparison. Bars show memory usage (red: 1-bit, green: 0.375-bit); lines indicate prefill latency across context lengths.

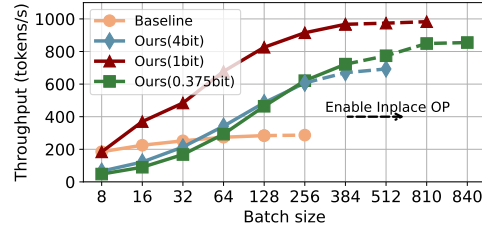


Figure 7: Decoding throughput comparison. Our method supports larger batch sizes and achieves higher throughput.

#### 4.5 Ablation Study

We conduct a series of experiments to answer the following questions.

**Q1: How does the model performance change as the number of anchor tokens increases?**

As the number of anchor tokens increases, the performance loss decreases rapidly at first, as shown in Table 1. However, the marginal benefit diminishes with more anchor tokens. Detailed results are provided in Appendix F.

**Q2: Does the calibration set affect the performance?**

We find that for VQ-based methods, the calibration set does have some impact on performance under low-bit settings. However, as shown in Table 1 (LLaMA-3-8B, 1-bit, C4), retaining anchor tokens effectively mitigates the performance drop caused by calibration set variation. More detailed results can be found in Appendix G.

## 5 Limitation & Conclusion

Although AnTKV demonstrates its advantages in experiments, it also has several limitations. First, more accurate AnS for tokens and higher performance implementations for its computation may be possible. AnTKV demonstrates strong potential in LLM serving by substantially reducing the size of the KV cache, which in turn alleviates I/O and memory constraints to a significant extent. Nevertheless, further empirical validation is required.

We observed from several experiments that different tokens exhibit varying sensitivity to KV quantization, which opens a new opportunity for a better memory-accuracy trade-off. To this end, we present AnTKV, a two-stage token-aware VQ framework that involves offline gradient weighted centroid learning and online anchor token selection guided by AnS. Moreover, to ensure the efficiency of AnTKV in LLM inference, we implement a lightweight GPU kernel compatible with FlashAttention to compute AnS with minimal overhead. Extensive experiments show that AnTKV achieves superior performance under low and ultra-low-bit quantization, significantly extending the maximum context length (up to 840K tokens) on a single A100 GPU while maintaining low perplexity and high throughput. Our results demonstrate the potential of token-aware quantization in scaling LLM inference to longer contexts without sacrificing accuracy.

## References

- [1] OpenAI. Gpt-4 technical report, 2023.
- [2] Daya Guo, Dejian Yang, Haowei Zhang, Junxiao Song, Ruoyu Zhang, Runxin Xu, Qihao Zhu, Shirong Ma, Peiyi Wang, Xiao Bi, et al. Deepseek-R1: Incentivizing reasoning capability in LLMs via reinforcement learning. *arXiv preprint arXiv:2501.12948*, 2025.
- [3] Gemini Team, Rohan Anil, Sebastian Borgeaud, Jean-Baptiste Alayrac, Jiahui Yu, Radu Soriccut, Johan Schalkwyk, Andrew M Dai, Anja Hauth, Katie Millican, et al. Gemini: a family of highly capable multimodal models. *arXiv preprint arXiv:2312.11805*, 2023.
- [4] Zhenheng Tang, Xiang Liu, Qian Wang, Peijie Dong, Bingsheng He, Xiaowen Chu, and Bo Li. The lottery LLM hypothesis, rethinking what abilities should LLM compression preserve? In *The Fourth Blogpost Track at ICLR 2025*, 2025.
- [5] Peijie Dong, Zhenheng Tang, Xiang Liu, Lujun Li, Xiaowen Chu, and Bo Li. Can compressed llms truly act? An empirical evaluation of agentic capabilities in LLM compression. In *Proceedings of the 42th International Conference on Machine Learning*, Proceedings of Machine Learning Research. PMLR, 2025.
- [6] Wayne Xin Zhao, Kun Zhou, Junyi Li, Tianyi Tang, Xiaolei Wang, Yupeng Hou, Yingqian Min, Beichen Zhang, Junjie Zhang, Zican Dong, et al. A survey of large language models. *arXiv preprint arXiv:2303.18223*, 1(2), 2023.
- [7] Qian Wang, Tianyu Wang, Zhenheng Tang, Qinbin Li, Nuo Chen, Jingsheng Liang, and Bingsheng He. MegaAgent: A large-scale autonomous LLM-based multi-agent system without predefined SOPs. In *The 63rd Annual Meeting of the Association for Computational Linguistics*, 2025.
- [8] Badhan Chandra Das, M Hadi Amini, and Yanzhao Wu. Security and privacy challenges of large language models: A survey. *ACM Computing Surveys*, 57(6):1–39, 2025.
- [9] Qian Wang, Zhenheng Tang, Zichen Jiang, Nuo Chen, Tianyu Wang, and Bingsheng He. AgentTaxo: Dissecting and benchmarking token distribution of LLM multi-agent systems. In *ICLR 2025 Workshop on Foundation Models in the Wild*, 2025.
- [10] Yuanbing Zhu, Zhenheng Tang, Xiang Liu, Ang Li, Bo Li, Xiaowen Chu, and Bo Han. OracleKV: Oracle guidance for question-independent KV cache compression. In *ICML 2025 Workshop on Long-Context Foundation Models*, 2025.
- [11] Yushi Bai, Xin Lv, Jiajie Zhang, Hongchang Lyu, Jiankai Tang, Zhidian Huang, Zhengxiao Du, Xiao Liu, Aohan Zeng, Lei Hou, Yuxiao Dong, Jie Tang, and Juanzi Li. LongBench: A bilingual, multitask benchmark for long context understanding. In *Proceedings of the 62nd Annual Meeting of the Association for Computational Linguistics (ACL)*, pages 3119–3137, 2024.

- [12] Jiaheng Liu, Dawei Zhu, Zhiqi Bai, Yancheng He, Huanxuan Liao, Haoran Que, Zekun Wang, Chenchen Zhang, Ge Zhang, Jiebin Zhang, et al. A comprehensive survey on long context language modeling. *arXiv preprint arXiv:2503.17407*, 2025.
- [13] Reiner Pope, Sholto Douglas, Aakanksha Chowdhery, Jacob Devlin, James Bradbury, Anselm Levskaya, Jonathan Heek, Kefan Xiao, Shivani Agrawal, and Jeff Dean. Efficiently scaling transformer inference, 2022.
- [14] Jiayi Yao, Hanchen Li, Yuhan Liu, Siddhant Ray, Yihua Cheng, Qizheng Zhang, Kuntai Du, Shan Lu, and Junchen Jiang. CacheBlend: Fast large language model serving for RAG with cached knowledge fusion. In *Proceedings of the Twentieth European Conference on Computer Systems, EuroSys '25*, page 94–109, New York, NY, USA, 2025. Association for Computing Machinery.
- [15] Xiang Liu, Zhenheng Tang, Peijie Dong, Zeyu Li, Bo Li, Xuming Hu, and Xiaowen Chu. ChunkKV: Semantic-preserving kv cache compression for efficient long-context LLM inference, 2025.
- [16] Xiang Liu, Zhenheng Tang, Hong Chen, Peijie Dong, Zeyu Li, Xiuze Zhou, Bo Li, Xuming Hu, and Xiaowen Chu. Can LLMs maintain fundamental abilities under KV cache compression?, 2025.
- [17] Di Liu, Meng Chen, Baotong Lu, Huiqiang Jiang, Zhenhua Han, Qianxi Zhang, Qi Chen, Chengruidong Zhang, Bailu Ding, Kai Zhang, et al. RetrievalAttention: Accelerating long-context LLM inference via vector retrieval. *arXiv preprint arXiv:2409.10516*, 2024.
- [18] Yuxin Zhang, Yuxuan Du, Gen Luo, Yunshan Zhong, Zhenyu Zhang, Shiwei Liu, and Rongrong Ji. CaM: cache merging for memory-efficient LLMs inference. In *Proceedings of the 41st International Conference on Machine Learning, ICML'24*. JMLR.org, 2024.
- [19] Zirui Liu, Jiayi Yuan, Hongye Jin, Shaochen Zhong, Zhaozhuo Xu, Vladimir Braverman, Beidi Chen, and Xia Hu. KIVI: A tuning-free asymmetric 2bit quantization for KV cache. In *International Conference on Machine Learning, ICML 2024*, pages 32332–32344. PMLR, 2024.
- [20] Haojie Duanmu, Zhihang Yuan, Xiuhong Li, Jiangfei Duan, Xingcheng Zhang, and Dahua Lin. SKVQ: Sliding-window key and value cache quantization for large language models, 2024.
- [21] Coleman Hooper, Sehoon Kim, Hiva Mohammadzadeh, Michael W Mahoney, Sophia Shao, Kurt Keutzer, and Amir Gholami. KVQuant: Towards 10 million context length LLM inference with KV cache quantization. *Advances in Neural Information Processing Systems, NeurIPS 2024*, 37:1270–1303, 2024.
- [22] Lucas D. Lingle. Transformer-VQ: Linear-time transformers via vector quantization, 2024.
- [23] Tianyi Zhang, Jonah Yi, Zhaozhuo Xu, and Anshumali Shrivastava. KV cache is 1 bit per channel: Efficient large language model inference with coupled quantization. *Advances in Neural Information Processing Systems, NeurIPS 2024*, 37:3304–3331, 2024.
- [24] Albert Q. Jiang, Alexandre Sablayrolles, Arthur Mensch, Chris Bamford, Devendra Singh Chaplot, et al. Mistral 7b, 2023.
- [25] Tri Dao. FlashAttention-2: Faster attention with better parallelism and work partitioning, 2023.
- [26] Hugo Touvron, Louis Martin, Kevin Stone, Peter Albert, Amjad Almahairi, et al. Llama 2: Open foundation and fine-tuned chat models, 2023.
- [27] Aaron Grattafiori, Abhimanyu Dubey, Abhinav Jauhri, Abhinav Pandey, Abhishek Kadian, et al. The Llama 3 herd of models, 2024.
- [28] Jianlin Su, Yu Lu, Shengfeng Pan, Ahmed Murtadha, Bo Wen, and Yunfeng Liu. Roformer: Enhanced transformer with rotary position embedding, 2023.
- [29] Jianlin Su, Murtadha Ahmed, Yu Lu, Shengfeng Pan, Wen Bo, and Yunfeng Liu. RoFormer: Enhanced transformer with rotary position embedding. *Neurocomputing*, 568:127063, 2024.

- [30] Qianchao Zhu, Jiangfei Duan, Chang Chen, Siran Liu, Xiuhong Li, Guanyu Feng, Xin Lv, Huanqi Cao, Chuanfu Xiao, Xingcheng Zhang, Dahua Lin, and Chao Yang. SampleAttention: Near-lossless acceleration of long context LLM inference with adaptive structured sparse attention. In *Ninth Annual Conference on Machine Learning and Systems, MLSys 2025*, 2025.
- [31] Guangxuan Xiao, Yuandong Tian, Beidi Chen, Song Han, and Mike Lewis. Efficient streaming language models with attention sinks. In *The Twelfth International Conference on Learning Representations, ICLR 2024*, 2024.
- [32] Mengzhao Chen, Yi Liu, Jiahao Wang, Yi Bin, Wenqi Shao, and Ping Luo. PrefixQuant: Static quantization beats dynamic through prefixed outliers in LLMs. *arXiv preprint arXiv:2410.05265*, 2024.
- [33] Yuhong Li, Yingbing Huang, Bowen Yang, Bharat Venkitesh, Acyr Locatelli, Hanchen Ye, Tianle Cai, Patrick Lewis, and Deming Chen. SnapKV: LLM knows what you are looking for before generation, 2024.
- [34] Zheng Wang, Boxiao Jin, Zhongzhi Yu, and Minjia Zhang. Model tells you where to merge: Adaptive KV cache merging for llms on long-context tasks, 2024.
- [35] Zhuoming Chen, Ranajoy Sadhukhan, Zihao Ye, Yang Zhou, Jianyu Zhang, Niklas Nolte, Yuandong Tian, Matthijs Douze, Leon Bottou, Zhihao Jia, et al. MagicPIG: LSH sampling for efficient LLM generation. In *Adaptive Foundation Models: Evolving AI for Personalized and Efficient Learning*, 2024.
- [36] Hailin Zhang, Xiaodong Ji, Yilin Chen, Fangcheng Fu, Xupeng Miao, Xiaonan Nie, Weipeng Chen, and Bin Cui. PQCache: Product quantization-based KVCache for long context LLM inference. *arXiv preprint arXiv:2407.12820*, 2024.
- [37] Elias Frantar, Saleh Ashkboos, Torsten Hoefler, and Dan Alistarh. GPTQ: Accurate post-training quantization for generative pre-trained transformers, 2023.
- [38] Guangxuan Xiao, Ji Lin, Mickael Seznec, Hao Wu, Julien Demouth, and Song Han. Smoothquant: Accurate and efficient post-training quantization for large language models, 2024.
- [39] Ji Lin, Jiaming Tang, Haotian Tang, Shang Yang, Wei-Ming Chen, Wei-Chen Wang, Guangxuan Xiao, Xingyu Dang, Chuang Gan, and Song Han. AWQ: Activation-aware weight quantization for LLM compression and acceleration, 2024.
- [40] Yifei Liu, Jicheng Wen, Yang Wang, Shengyu Ye, Li Lyna Zhang, Ting Cao, Cheng Li, and Mao Yang. VPTQ: Extreme low-bit vector post-training quantization for large language models, 2024.
- [41] Albert Tseng, Jerry Chee, Qingyao Sun, Volodymyr Kuleshov, and Christopher De Sa. Quip#: Even better llm quantization with hadamard incoherence and lattice codebooks, 2024.
- [42] Yilong Zhao, Chien-Yu Lin, Kan Zhu, Zihao Ye, Lequn Chen, Size Zheng, Luis Ceze, Arvind Krishnamurthy, Tianqi Chen, and Baris Kasikci. Atom: Low-bit quantization for efficient and accurate LLM serving, 2024.
- [43] Yujun Lin, Haotian Tang, Shang Yang, Zhekai Zhang, Guangxuan Xiao, Chuang Gan, and Song Han. QServe: W4A8KV4 quantization and system co-design for efficient LLM serving, 2025.
- [44] Peijie Dong, Lujun Li, Zhenheng Tang, Xiang Liu, Xinglin Pan, Qiang Wang, and Xiaowen Chu. Pruner-Zero: Evolving symbolic pruning metric from scratch for large language models, 2024.
- [45] Peijie Dong, Lujun Li, Xinglin Pan, Zimian Wei, Xiang Liu, Qiang Wang, and Xiaowen Chu. Parzc: Parametric zero-cost proxies for efficient nas, 2024.
- [46] Haojun Xia, Zhen Zheng, Yuchao Li, Donglin Zhuang, Zhongzhu Zhou, Xiafei Qiu, Yong Li, Wei Lin, and Shuaiwen Leon Song. Flash-LLM: Enabling cost-effective and highly-efficient large generative model inference with unstructured sparsity, 2023.

- [47] Ruibo Fan, Xiangrui Yu, Peijie Dong, Zeyu Li, Gu Gong, Qiang Wang, Wei Wang, and Xiaowen Chu. Spinfer: Leveraging low-level sparsity for efficient large language model inference on gpus. In *Proceedings of the Twentieth European Conference on Computer Systems*, EuroSys '25, page 243–260, New York, NY, USA, 2025. Association for Computing Machinery.
- [48] Dan Hendrycks, Collin Burns, Steven Basart, Andy Zou, Mantas Mazeika, Dawn Song, and Jacob Steinhardt. Measuring massive multitask language understanding, 2021.
- [49] Peter Clark, Isaac Cowhey, Oren Etzioni, Tushar Khot, Ashish Sabharwal, Carissa Schoenick, and Oyvind Tafjord. Think you have solved question answering? Try ARC, the AI2 reasoning challenge. *arXiv preprint arXiv:1803.05457*, 2018.
- [50] Aida Amini, Saadia Gabriel, Shanchuan Lin, Rik Koncel-Kedziorski, Yejin Choi, and Hannaneh Hajishirzi. MathQA: Towards interpretable math word problem solving with operation-based formalisms. In *Proceedings of the 2019 Conference of the North American Chapter of the Association for Computational Linguistics: Human Language Technologies*, pages 2357–2367, 2019.
- [51] Yonatan Bisk, Rowan Zellers, Ronan Le Bras, Jianfeng Gao, and Yejin Choi. PIQA: Reasoning about physical commonsense in natural language. In *Proceedings of the AAAI Conference on Artificial Intelligence*, volume 34, pages 7432–7439, 2020.

## A Distribution of pre- and post- RoPE Key

To identify a quantization strategy better suited for  $K$  vector quantization, we compare the distribution of  $K$  before and after applying RoPE. Figure 8 presents a visualization of the pre- and post-RoPE  $K$ . We observe that, compared to the post-RoPE  $K$ , the pre-RoPE  $K$  exhibits smaller inter-cluster distances and lower intra-cluster variance, which contributes to reduced quantization error.

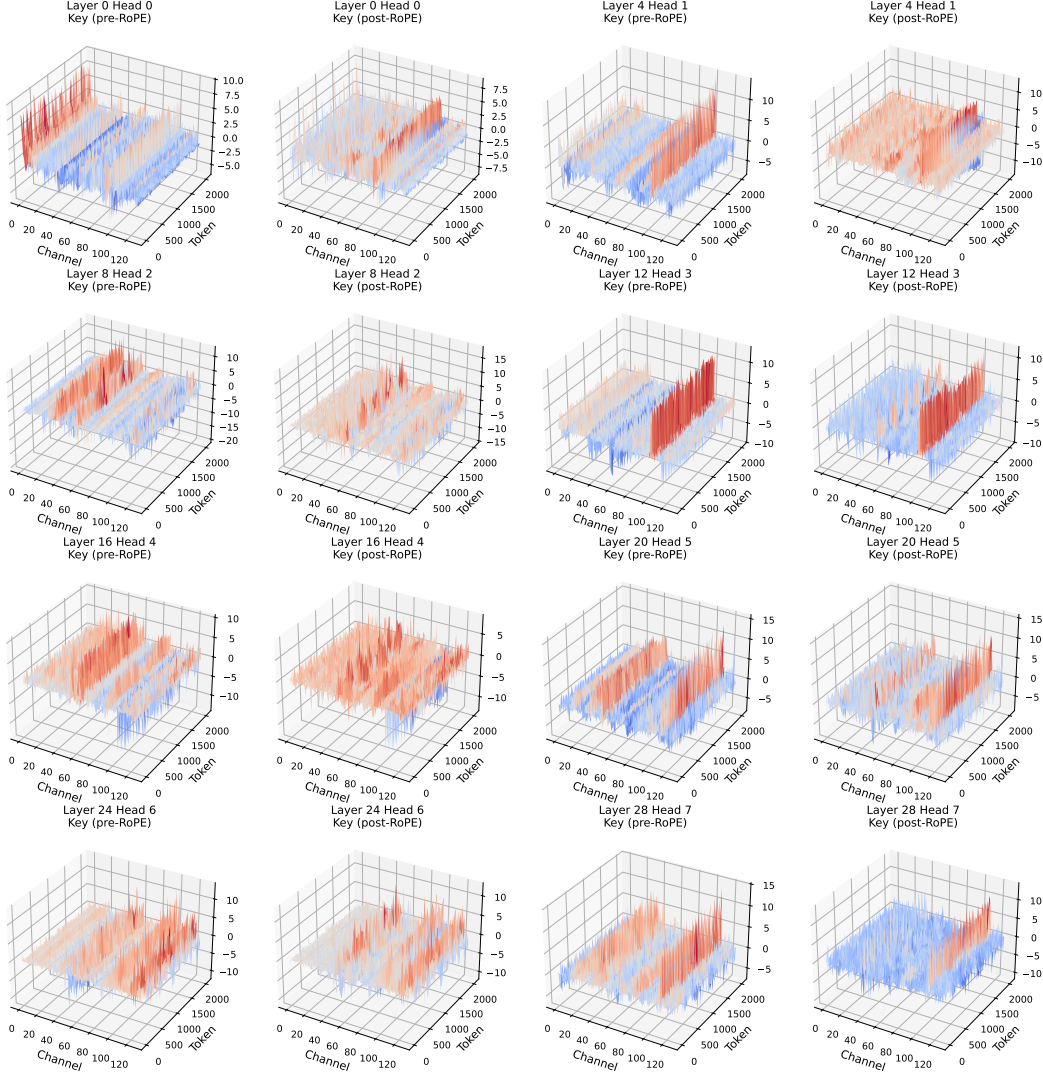


Figure 8: Distribution of pre- and post- RoPE Key. We sampled a 2048-length sentence from WikiText2 and generated pre- and post- RoPE Key on the LLaMA-3-8B model.

## B Proof of Theorem 3.1

For  $K$ , we have

$$\|\text{Attn}(Q, K + \delta K, V) - \text{Attn}(Q, K, V)\|_{L_1} = \left\| \left( \text{Softmax} \left( \frac{\tilde{Q}\tilde{K}^T}{\sqrt{d}} + \frac{\tilde{Q}\delta\tilde{K}^T}{\sqrt{d}} \right) - \text{Softmax} \left( \frac{\tilde{Q}\tilde{K}^T}{\sqrt{d}} \right) \right) V \right\|_{L_1}. \quad (6)$$

The key to estimating the bound of (6) lies in the analysis of

$$\text{Softmax} \left( \frac{\tilde{Q}\tilde{K}^T}{\sqrt{d}} + \frac{\tilde{Q}\delta\tilde{K}^T}{\sqrt{d}} \right) - \text{Softmax} \left( \frac{\tilde{Q}\tilde{K}^T}{\sqrt{d}} \right), \quad (7)$$

whose  $(i, j)$ th entry is represented as

$$\frac{\exp\left(\frac{\tilde{Q}_{i,:}\tilde{K}_{j,:}^T}{\sqrt{d}} + \frac{\tilde{Q}_{i,:}\delta\tilde{K}_{j,:}^T}{\sqrt{d}}\right)}{\sum_s \exp\left(\frac{\tilde{Q}_{i,:}\tilde{K}_{s,:}^T}{\sqrt{d}} + \frac{\tilde{Q}_{i,:}\delta\tilde{K}_{s,:}^T}{\sqrt{d}}\right)} - \frac{\exp\left(\frac{\tilde{Q}_{i,:}\tilde{K}_{j,:}^T}{\sqrt{d}}\right)}{\sum_s \exp\left(\frac{\tilde{Q}_{i,:}\tilde{K}_{s,:}^T}{\sqrt{d}}\right)}. \quad (8)$$

Since  $\|\delta\mathbf{K}\|_{L_1} \ll \|\mathbf{K}\|_{L_1}$ , and by the first-order approximation  $\exp(x + \delta x) \approx \exp(x)(1 + \delta x)$ , (8) can be approximated as

$$\begin{aligned} & \frac{\exp\left(\frac{\tilde{Q}_{i,:}\tilde{K}_{j,:}^T}{\sqrt{d}}\right) \left(1 + \frac{\tilde{Q}_{i,:}\delta\tilde{K}_{j,:}^T}{\sqrt{d}}\right) \left(\sum_s \exp\left(\frac{\tilde{Q}_{i,:}\tilde{K}_{s,:}^T}{\sqrt{d}}\right)\right) - \exp\left(\frac{\tilde{Q}_{i,:}\tilde{K}_{j,:}^T}{\sqrt{d}}\right) \left(\sum_s \exp\left(\frac{\tilde{Q}_{i,:}\tilde{K}_{s,:}^T}{\sqrt{d}}\right) \left(1 + \frac{\tilde{Q}_{i,:}\delta\tilde{K}_{s,:}^T}{\sqrt{d}}\right)\right)}{\left(\sum_s \exp\left(\frac{\tilde{Q}_{i,:}\tilde{K}_{s,:}^T}{\sqrt{d}}\right)\right) \left(\sum_s \exp\left(\frac{\tilde{Q}_{i,:}\tilde{K}_{s,:}^T}{\sqrt{d}}\right) \left(1 + \frac{\tilde{Q}_{i,:}\delta\tilde{K}_{s,:}^T}{\sqrt{d}}\right)\right)} \\ &= \frac{\exp\left(\frac{\tilde{Q}_{i,:}\tilde{K}_{j,:}^T}{\sqrt{d}}\right)}{\sum_s \exp\left(\frac{\tilde{Q}_{i,:}\tilde{K}_{s,:}^T}{\sqrt{d}}\right)} \cdot \frac{\sum_s \exp\left(\frac{\tilde{Q}_{i,:}\tilde{K}_{s,:}^T}{\sqrt{d}}\right) \left(\frac{\tilde{Q}_{i,:}(\delta\tilde{K}_{j,:}^T - \delta\tilde{K}_{s,:}^T)}{\sqrt{d}}\right)}{\sum_s \exp\left(\frac{\tilde{Q}_{i,:}\tilde{K}_{s,:}^T}{\sqrt{d}}\right) \left(1 + \frac{\tilde{Q}_{i,:}\delta\tilde{K}_{s,:}^T}{\sqrt{d}}\right)} \\ &\approx \frac{\exp\left(\frac{\tilde{Q}_{i,:}\tilde{K}_{j,:}^T}{\sqrt{d}}\right)}{\sum_s \exp\left(\frac{\tilde{Q}_{i,:}\tilde{K}_{s,:}^T}{\sqrt{d}}\right)} \cdot \frac{\sum_s \exp\left(\frac{\tilde{Q}_{i,:}\tilde{K}_{s,:}^T}{\sqrt{d}}\right) \left(\frac{\tilde{Q}_{i,:}(\delta\tilde{K}_{j,:}^T - \delta\tilde{K}_{s,:}^T)}{\sqrt{d}}\right)}{\sum_s \exp\left(\frac{\tilde{Q}_{i,:}\tilde{K}_{s,:}^T}{\sqrt{d}}\right)} \\ &= \mathbf{A}_{i,j} \cdot \frac{\sum_s \exp\left(\frac{\tilde{Q}_{i,:}\tilde{K}_{s,:}^T}{\sqrt{d}}\right) \left(\frac{\tilde{Q}_{i,:}(\delta\tilde{K}_{j,:}^T - \delta\tilde{K}_{s,:}^T)}{\sqrt{d}}\right)}{\sum_s \exp\left(\frac{\tilde{Q}_{i,:}\tilde{K}_{s,:}^T}{\sqrt{d}}\right)}. \end{aligned}$$

For convenience, we denote  $\frac{\tilde{Q}\delta\tilde{K}^T}{\sqrt{d}}$  and  $\left[\frac{\sum_s \exp\left(\frac{\tilde{Q}_{i,:}\tilde{K}_{s,:}^T}{\sqrt{d}}\right) \left(\frac{\tilde{Q}_{i,:}(\delta\tilde{K}_{j,:}^T - \delta\tilde{K}_{s,:}^T)}{\sqrt{d}}\right)}{\sum_s \exp\left(\frac{\tilde{Q}_{i,:}\tilde{K}_{s,:}^T}{\sqrt{d}}\right)}\right]_{n \times n}$  as  $\mathbf{X}$  and  $\mathbf{Y}$

respectively. Then (7) can be approximated as  $(\mathbf{A} \odot \mathbf{Y})\mathbf{V}$ , and by the property of Kronecker product, we have

$$\text{Vec}((\mathbf{A} \odot \mathbf{Y})\mathbf{V}) = (\mathbf{I}_n \otimes \mathbf{V}^T) \text{Vec}(\mathbf{A} \odot \mathbf{Y}) = (\mathbf{I}_n \otimes \mathbf{V}^T) \text{Diag}(\text{Vec}(\mathbf{A})) \text{Vec}(\mathbf{Y}).$$

Further, we can obtain

$$\begin{aligned} \|\text{Attn}(\mathbf{Q}, \mathbf{K} + \delta\mathbf{K}, \mathbf{V}) - \text{Attn}(\mathbf{Q}, \mathbf{K}, \mathbf{V})\|_{L_1} &\approx \|(\mathbf{I}_n \otimes \mathbf{V}^T) \text{Diag}(\text{Vec}(\mathbf{A})) \text{Vec}(\mathbf{Y})\|_{L_1} \\ &= \sum_i \|\mathbf{V}^T \text{Diag}(\mathbf{A}_{i,:}) (\mathbf{I}_n - \mathbf{e}\mathbf{A}_{i,:}) \mathbf{X}_{i,:}^T\|_{L_1} \\ &\leq \sum_i \sum_j \|\left(\mathbf{V}^T \text{Diag}(\mathbf{A}_{i,:}) (\mathbf{I}_n - \mathbf{e}\mathbf{A}_{i,:})\right)_{:,j}\|_{L_1} |\tilde{Q}_{i,:}\delta\tilde{K}_{j,:}^T| \\ &\leq \sum_j \sum_i \|\left(\mathbf{V}^T \text{Diag}(\mathbf{A}_{i,:}) (\mathbf{I}_n - \mathbf{e}\mathbf{A}_{i,:})\right)_{:,j}\|_{L_1} \|\mathbf{Q}_{i,:}\|_2 \|\delta\mathbf{K}_{j,:}\|_{L_1}. \end{aligned} \quad (9)$$

For  $\mathbf{V}$ , we have

$$\begin{aligned} \|\text{Attn}(\mathbf{Q}, \mathbf{K}, \mathbf{V} + \delta\mathbf{V}) - \text{Attn}(\mathbf{Q}, \mathbf{K}, \mathbf{V})\|_{L_1} &= \|\text{Softmax}\left(\frac{\tilde{Q}\tilde{K}^T}{\sqrt{d}}\right) \delta\mathbf{V}\|_{L_1} \\ &= \|\mathbf{A}\delta\mathbf{V}\|_{L_1} = \sum_{i,k} \left| \sum_j \mathbf{A}_{i,j} \delta\mathbf{V}_{j,k} \right| \\ &\leq \sum_{i,k} \sum_j \mathbf{A}_{i,j} |\delta\mathbf{V}_{j,k}| \\ &= \sum_j \left( \sum_i \mathbf{A}_{i,j} \right) \left( \sum_k |\delta\mathbf{V}_{j,k}| \right) \\ &= \sum_j \|\mathbf{A}_{:,j}\|_{L_1} \|\delta\mathbf{V}_{j,:}\|_{L_1}. \end{aligned} \quad (10)$$

## C The Effectiveness of AnS

We quantized each token across layers and heads, and separately recorded the errors in the attention outputs. As shown in Figure 9 and (5), it can be observed that the relative values derived from our AnS, as defined in Theorem 3.1, closely align with the actual outputs of the attention. For a fair comparison, the output errors for  $\mathbf{K}$  also exclude the contribution of  $\mathbf{V}$ .

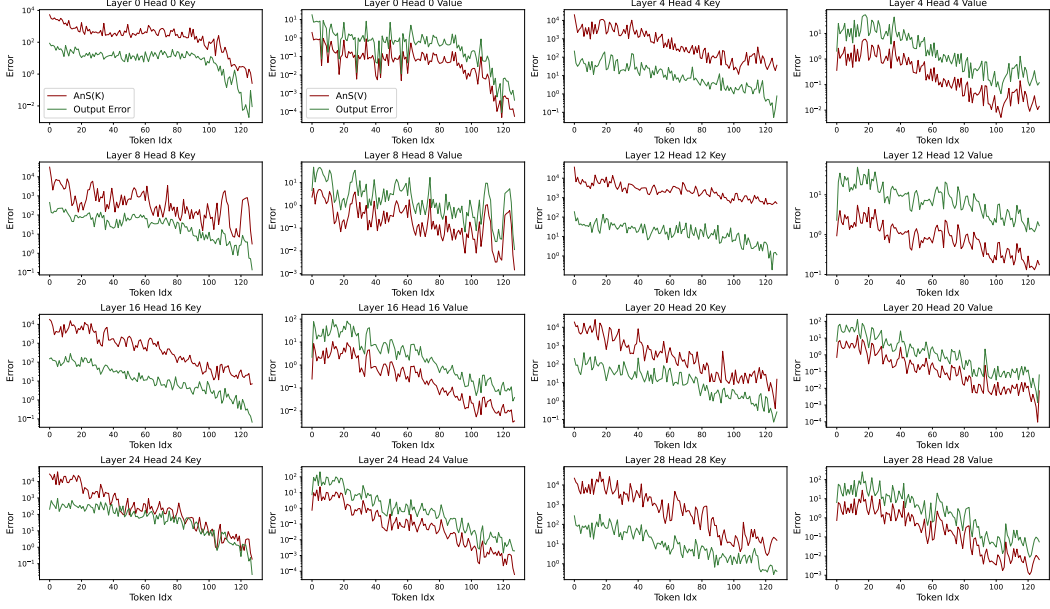


Figure 9: The effectiveness of AnS.

## D AnS Distribution During Decoding

To illustrate the distribution of AnS during decoding, we sampled prompts from Qasper within LongBench for visualization. As shown in Figure 10, we present the distribution of  $\text{AnS}(\mathbf{K})$  and  $\text{AnS}(\mathbf{V})$  across different layers and heads, specifically when decoding the first token. Our observations reveal that high AnS values during decoding are predominantly concentrated on adjacent tokens and at the attention sink tokens. Since sink tokens often lead to significant error propagation and can be dynamically identified by AnS during prefill, we simplify the design of AnS during decoding by employing a sliding window to ensure model performance.

## E Computational Procedure of AnS in the Online Stage

---

**Algorithm 1** The computation of AnS in the online stage.

---

- 1: **Input:** Query ( $\mathbf{Q}$ ), key ( $\mathbf{K}$ ), value ( $\mathbf{V}$ )
  - 2: **Output:** AnS of KV, i.e.,  $\text{AnS}(\mathbf{K})$  and  $\text{AnS}(\mathbf{V})$
  - 3:  $(\mathbf{O}, \mathbf{L}, \mathbf{M}, \|\mathbf{Q}_{i,:}\|_{L_2}) \leftarrow \text{FlashAttention}(\mathbf{Q}, \mathbf{K}, \mathbf{V})$
  - 4: **for** each block key index  $j$  in parallel (assigned to GPU block) **do**
  - 5:     **for** each block query index  $i$  **do**
  - 6:          $\mathbf{S}_{i,j} \leftarrow \langle \mathbf{Q}_{h,i}, \mathbf{K}_{h,j} \rangle$
  - 7:          $\mathbf{A}_{i,j} \leftarrow \exp(\mathbf{S}_{i,j} - \mathbf{M}_{h,i}) / \mathbf{L}_{h,i}$
  - 8:          $\text{AnS}(\mathbf{K})_i \leftarrow \text{AnS}(\mathbf{K})_i + \text{col\_sum}(\mathbf{A}_{i,j} \cdot (1 - \mathbf{A}_{i,j}), \text{row-wise})$
  - 9:          $\text{AnS}(\mathbf{V})_i \leftarrow \text{AnS}(\mathbf{V})_i + \text{col\_sum}(\mathbf{A}_{i,j}, \text{row-wise})$
  - 10:     **end for**
  - 11: **end for**
  - 12: **return**  $\text{AnS}(\mathbf{K}), \text{AnS}(\mathbf{V})$
-

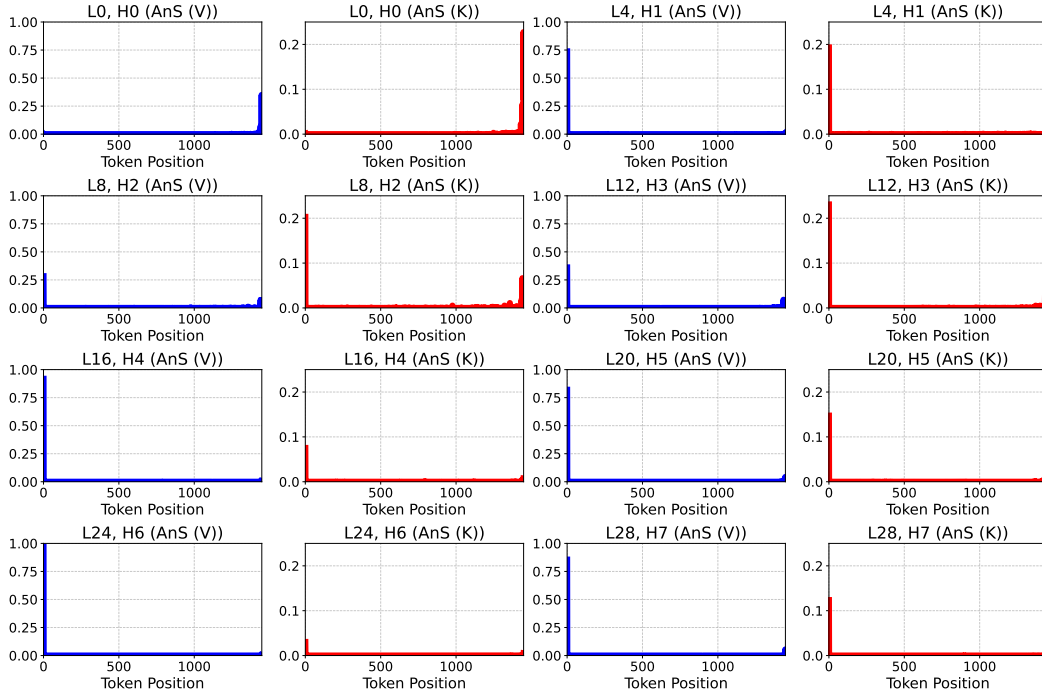


Figure 10: AnS Distribution on Sampled Prompts from Qasper Using LLaMA-3-8B-Instruct During First-Token Decoding.

## F Calibration Set Impact

As shown in the Table 2, we observe that for VQ-based quantization in the ultra-low-bit regime, the calibration set significantly impacts the perplexity results. However, AnTKV with 1% anchor tokens not only substantially reduces the PPL but also greatly mitigates the effect of different calibration sets.

Table 2: Perplexity experiment results on Mistral-7B, using the W2 and C4 training sets respectively as Calibration Sets. The "Vset" is the validation set related to W2 and C4. "Calib Set" represents "Calibration Set".

Bits	Vset	4		2		1		0.75		0.375	
Calib Set		W2	C4	W2	C4	W2	C4	W2	C4	W2	C4
Ours	W2	4.76	5.69	5.08	6.18	7.32	10.51	7.32	10.51	11.65	23.98
	C4	4.79	5.69	5.32	6.15	10.14	10.09	10.90	10.80	24.16	19.95
Ours-1%	W2	4.74	5.67	4.95	5.97	6.32	8.44	6.32	8.44	8.87	14.87
	C4	4.75	5.66	5.02	5.94	7.13	8.13	7.79	8.56	12.87	13.07

To further investigate the impact of the calibration set on model performance, we used C4 as a calibration set to evaluate several subtasks within LongBench (qasper, trec, samsun, lcc, ropebench-p). As shown in the Table 3, we observed that there were some differences in the results of Trec and Repobench-p when using Wikitext-2 and C4, while the differences were not significant for the other tasks.

Table 3: Performance on LongBench Subtasks with Wikitext-2 (W2) and C4 Calibration Sets at Different Bits using LLaMA-3-8B-Instruct. "Calib Set" represents "Calibration Set", and "repopc-p" represents "repopbench-p".

Bits	4		2		1		0.75		0.375	
Calib Set	W2	C4								
gasper	40.46	39.98	39.04	38.2	25.95	26.51	25.48	25.49	22.41	23.27
trec	69.33	69.33	67	64.67	38.67	42.33	39.67	41.33	38	38
samsun	40.2	40.27	38.61	38.22	30.0	30.3	29.57	29.29	25.5	24.82
lcc	59.84	59.07	60.94	59.15	53.97	53.93	52.97	52.01	49.61	49.79
repopc-p	44.24	41.3	45.29	42.68	38.53	37.94	37.87	38.02	34.54	34.71

## G Anchor Tokens Number Impact

To investigate the impact of the number of anchor tokens on model performance, we conducted Perplexity evaluations on Mistral-7B and LLaMA-3-8B, both with a context length of 8192. We performed evaluations using no anchor tokens and with anchor token percentages of 1% (82), 2% (164), 5% (410), 10% (820), 15% (1230), and 20% (1640). The corresponding results are presented in Figures 11 and 12. For the 2-bit and 4-bit results, using 1% of anchor tokens kept the error within 0.6 compared to FP16. However, for the 1-bit and sub-bit results, we needed to increase the number of anchor tokens to control the error within an acceptable range. Nevertheless, AnTKV provides a feasible technical pathway for ultra-low-bit quantization of the KV cache.

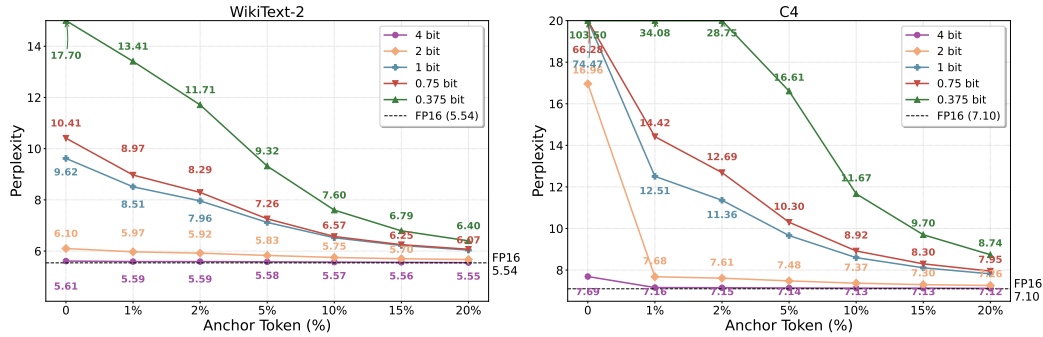


Figure 11: Perplexity results on LLaMA-3-8B with varying anchor token numbers.

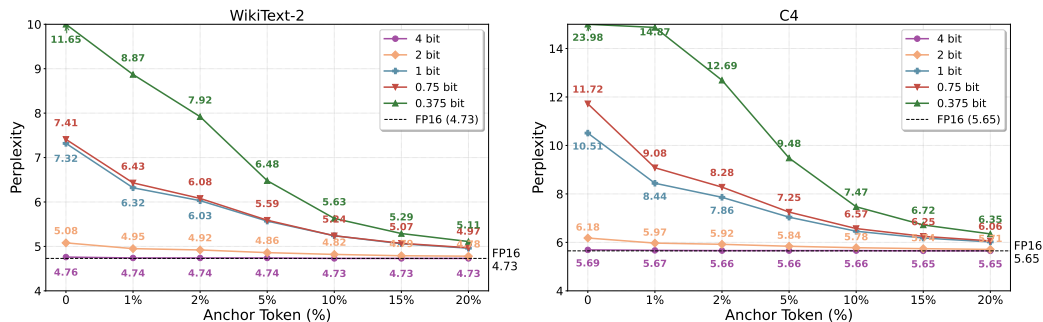


Figure 12: Perplexity results on Mistral-7B with varying anchor token numbers.

To further investigate the impact of anchor token numbers on downstream tasks, we evaluated different anchor token numbers on the Trec and Qasper subtasks of LongBench under ultra-low-bit quantization settings. For convenience, we approximated 1% of the anchor token number as 64. The

results are shown in Figure 13. The results indicate that Trec’s performance increases linearly with the number of anchor tokens, eventually reaching a result within 10 points of the baseline when using 10% anchor tokens. In contrast to Trec, Qasper’s accuracy remains stable with a small number of anchor tokens but shows a significant performance improvement when increased to 10%. We believe this difference stems from the inherent properties of each task.

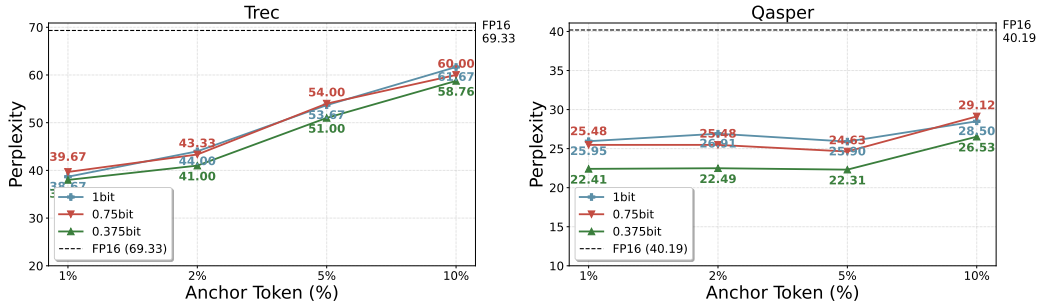


Figure 13: Trec and Qasper results on LLaMA-3-8B-Instruct with varying anchor token numbers.

## H Models, Datasets and Code

### H.1 Models Checkpoints

Here, we list all of the model checkpoints used in our experiments.

- LLaMA-2-7b <https://huggingface.co/meta-llama/Llama-2-7b>
- LLaMA-3-8B <https://huggingface.co/meta-llama/Meta-Llama-3-8B>
- LLaMA-3-8B-Instruct <https://huggingface.co/meta-llama/Meta-Llama-3-8B-Instruct>
- Mistral-7B <https://huggingface.co/mistralai/Mistral-7B-v0.1>
- Mistral-7B-Instruct <https://huggingface.co/mistralai/Mistral-7B-Instruct-v0.3>

### H.2 Datasets

- WikiText2 <https://huggingface.co/datasets/mindchain/wikitext2>
- C4 <https://huggingface.co/datasets/allenai/c4>
- MMLU <https://huggingface.co/datasets/cais/mmlu>
- ARC-C [https://huggingface.co/datasets/allenai/ai2\\_arc](https://huggingface.co/datasets/allenai/ai2_arc)
- PIQA <https://huggingface.co/datasets/ybisk/piqa>
- MathQA [https://huggingface.co/datasets/allenai/math\\_qa](https://huggingface.co/datasets/allenai/math_qa)
- LongBench <https://huggingface.co/datasets/THUDM/LongBench>

### H.3 Code

Our code and the trained centroids will be publicly released upon the acceptance of this paper.

## I Broader Impact

In this work, we observe that tokens in the KV cache exhibit heterogeneous sensitivity to quantization, an insight that challenges the prevailing assumption of uniform importance across tokens. This observation paves the way for a new paradigm of importance-aware compression in LLMs. Our proposed method, AnTKV, embodies this paradigm through a two-stage, token-aware token quantization

framework. By selectively preserving high-impact tokens, AnTKV achieves strong performance even under ultra-low-bit quantization. Given its effectiveness and compatibility with high-throughput inference, AnTKV holds the potential to be widely adopted in future LLM compression and deployment practices.